

# Lowering the C-H Bond Activation Barrier of Methane Using SAC@Cu(111): A Periodic DFT Investigations

Meema Bhati,<sup>†,‡</sup> Jignesh Dhumal,<sup>†</sup> and Kavita Joshi<sup>\*,†,‡</sup>

<sup>†</sup>*Physical and Materials Chemistry Division, CSIR-National Chemical Laboratory, Dr. Homi Bhabha Road, Pune-411008, India.*

<sup>‡</sup>*Academy of Scientific and Innovative Research (AcSIR), Ghaziabad-201002, India.*

E-mail: k.joshi@ncl.res.in

## Abstract

Methane has long captured the world's spotlight for being the simplest and yet one of the most notorious hydrocarbon. Exploring its potential to be converted into value-added products has raised a compelling interest. In the present work, we have studied the efficiency of Single-Atom Catalysts (SACs) for methane activation employing Density Functional Theory (DFT). The Climbing Image-Nudged Elastic Band (CI-NEB) method is used in tandem with the Improved Dimer (ID) method to determine the minimum energy pathway for the first C-H bond dissociation of methane. Our study reported that the transition-metal doped Cu(111) surfaces enhance adsorption, activate C-H bond, and reduce activation barrier for first C-H bond cleavage of methane. The results suggest Ru/Co/Rh doped Cu(111) as promising candidates for methane activation with minimal activation barrier and less endothermic reaction. For these SACs, the calculated activation barriers for first C-H bond cleavage are 0.17 eV, 0.24 eV, and

0.26 eV respectively, which is substantially lower than 1.13 eV, the activation barrier for Cu(111).

## Introduction

Earth is home to rich reserves of methane, making it an attractive feedstock and a foremost competitor for the production of green fuel.<sup>1</sup> The myriad occurrence of methane can be attributed to its stable nature. Higher symmetry (Td) along with close shell electronic configuration, wide HOMO-LUMO gap ( $\approx 8.9$  eV), and four stable C-H bonds ( $E_{bd} \approx 4.5$  eV), makes it thermodynamically and kinetically stable at room temperature. Given the significant mass percentage of hydrogen (25.13%) in methane, it is widely used for hydrogen production.<sup>2</sup> Steam Methane Reforming (SMR) and Fischer-Tropsch (FT) synthesis are widely used processes for conversion of methane to hydrogen as well as to value-added products like methanol, formic acid, formaldehyde, higher hydrocarbons, and FT fuels. However, stability of methane makes it resistant to electrophilic and nucleophilic attacks. For most methane conversion reactions, the first C-H bond cleavage is the primary and the rate-limiting step. This motivates the rational design of a catalyst aiming at reducing the activation barrier for C-H bond dissociation.

Planar and stepped nickel surfaces are go-to catalysts used industrially in the aforementioned processes, primarily because Ni is procured at cheap rates and portrays excellent reactivity towards methane. The drawback of Ni catalysts is that they can completely dehydrogenate methane into carbon and hydrogen, which causes coking. Nullifying or preventing coking in methane conversion reactions is challenging area of current research.<sup>3,4</sup> The literature cites multiple studies in both theoretical and experimental verticals across various catalyst classes discussing methane activation. For example, it has been investigated on supported metal clusters,<sup>5</sup> noble metal surfaces,<sup>6-9</sup> mixed-metal alloys,<sup>10</sup> zeolites,<sup>11</sup> metal-organic frameworks(MOFs),<sup>12</sup> metal oxides,<sup>13-15</sup> perovskite,<sup>16</sup> and supported single-atom

catalysts (SACs)<sup>17</sup> to name a few. Lately, SACs have emerged as a focal point in active research surrounding methane activation.<sup>13,16,18</sup> Doping the base metal with a single atom increases the number of active sites on the surface, thus reducing the use of precious metals as traditional catalysts. SACs, as an interesting class of catalyst subtly modify the electronic structure of the base metal and the dopant itself. This unique alteration of properties is a consequence of changing the atomic environment and dopant-doped interaction. Pt doped rutile TiO<sub>2</sub>(110) catalyst ( $E_{ads} = -0.62$  eV,  $E_{act} = 0.15$  eV)<sup>13</sup> and Ag-doped CeO<sub>2</sub>(100)( $E_{ads} = -1.01$  eV,  $E_{act} = 0.21$  eV)<sup>14</sup> have shown considerable activity in terms of bondlength activation, adsorption energy, and activation barrier. IrO<sub>2</sub>(110) activates methane at low temperature,<sup>19</sup> and IrO<sub>2</sub> nanoparticles activate it at temperatures as low as 110<sup>0</sup>C.<sup>20</sup> Pt@SrBO<sub>3</sub> (100) surfaces (where B = Ti, V, and Cr transition metals) chemisorb methane dissociatively,<sup>16</sup> are also some prominent examples from the literature.

The work presented here is focused on the study of methane activation, in particular the adsorption, C-H bond elongation, and the C-H bond dissociation over several M@Cu(111). The Transition State (TS) analysis is performed for potent SACs where maximum bond elongation and adsorption is observed, using the CI-NEB and ID method. The metal atom interacts weakly with CH<sub>4</sub> molecule if it's d-orbitals are filled, whereas strong interaction occurs when d-orbitals are partially filled. Ru, Co, and Rh/Cu(111) show better chemical reactivity towards methane dissociation, where activation barrier is found to be much lower than that of Cu(111) surface. Our calculations provide atomic level insights into the mechanism of methane activation on SACs, and identify Ru/Co/Rh doped Cu(111) as a potent catalyst for first C-H bond dissociation.

## Computational Details

Kohn-Sham Formalism of Density Functional Theory (DFT) is employed to carry out all the calculations. Projector Augmented Wave potential is used,<sup>21,22</sup> with Perdew-Burke-

Ernzerhof (PBE)<sup>23</sup> approximation for the exchange-correlation and generalized gradient approximation<sup>24</sup> as implemented in plane-wave, pseudopotential based code, Vienna Ab-initio Simulation Package (VASP).<sup>25-27</sup> Within our framework, the calculated value of the lattice constant for Cu is found to be 3.62 Å which is in agreement with the experimental value of 3.61 Å.<sup>28</sup> Atomic Simulation Environment (ASE)<sup>29</sup> is used to cleave Cu(111) surface. We substituted one of the Cu surface atom with the dopant to model the SACs under investigation. We used a 3x3x4 supercell with a 5x5x1 Monkhorst Pack grid resulting into 13 K-points in the IBZ for primary screening of twenty-two SACs towards methane adsorption. The k-points convergence exercise was carried out by increasing the Monkhorst-Pack grid for each system. It was observed that the difference in energies was less than 4 meV/atom for every system. Ten potential candidates were then investigated for first C-H bond cleavage, in a 4x4x4 supercell with a 3x3x1 Monkhorst Pack grid. Our calculations reported that a change in system setup is not associated with any observable changes in adsorption energies and bondlength activation. 24 Å of vacuum is found to be sufficient to avoid interaction between adjacent images of planes along the z-direction. The criteria of a force cutoff of 0.01 eV/Å on the unfixed atoms and the total energy convergence below 10<sup>-5</sup> eV for each SCF cycle are employed for geometry optimization. The Van der Waals corrections are applied to all the calculations. The adsorption energy ( $E_{ads}$ ) is calculated as,  $E_{ads} = E_{slab+methane} - (E_{slab} + E_{methane})$ ; where  $E_{slab+methane}$  is the energy of the system when methane is placed on the slab,  $E_{slab}$  is the energy of the bare slab,  $E_{methane}$  is the energy of the methane molecule. A negative value of  $E_{ads}$  indicates an exothermic chemisorption process. Methane decomposition ( $CH_4 \rightarrow CH_3 + H$ ) reaction is studied by employing Climbing Image - Nudged Elastic Band (CI-NEB) method<sup>30</sup> and Improve Dimer (ID) method<sup>31,32</sup> and activation barriers are reported. Three images are considered for TS calculations using a force convergence of 0.1 eV/Å. The transition state structure is confirmed by vibrational frequency analysis, and zero point energy correction is applied in all the cases. Projected Density of States (*pDOS*) are calculated with denser k-mesh using LOBSTER<sup>33-36</sup> to understand the site-specific ad-

sorption pattern. Finally, Mulliken charges are calculated for all the atoms on the surface, providing insights into the quantitative charge transfer.

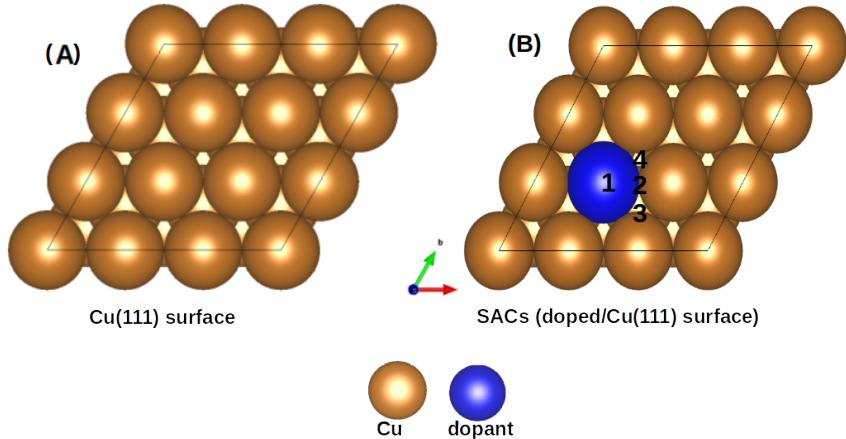


Figure 1: Top view of the unit cells: (a) Cu(111), (b) TM/Cu(111) surface. 1,2,3, and 4 represent the unique adsorption sites

## Results and discussions

Copper is an economically viable resource, while its (111) facet is naturally abundant. Our choice of copper as the base metal largely revolved around the fact that it prevents over-oxidation of products, portrays improved selectivity, and is resistant to coking. Twenty-two dopants are doped on a Cu(111) model system. The dopants chosen are well studied and are known to form alloys with copper.<sup>37</sup> The single-atom site was alloyed in Cu(111) surface to create a Single-Atom Catalyst (SAC). Eighteen of the dopants belong to transition metals vis-a-vis; Ti, V, Cr, Mn, Fe, Co, Ni, Zn of 3d series, Zr, Mo, Tc, Ru, Rh, Pd, Ag from 4d series, and Ir, Pt, Au belonging to 5d series. The remaining four Al, Mg, Pb, and Bi are non-transition metals. SACs doped with non-transition metals do not show C-H bond activation and hence the results and discussions henceforth only include TM@Cu(111). Four unique adsorption sites are recognized for methane adsorption on the SACs and are shown in Fig. 1. Adsorption of methane on SACs is analyzed based on C-H bond elongation, variation

in bond angles, alterations to M-C bondlength, and adsorption energies.

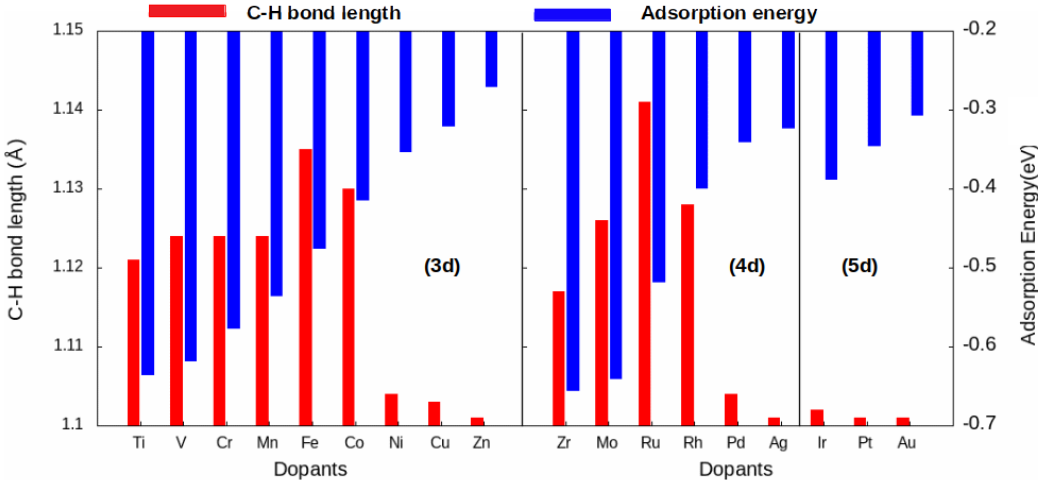


Figure 2: C-H bondlength activation (red, left y-axis) and adsorption energies (blue, right y-axis) are plotted as a function of dopant. Correlation between adsorption energies and group of the dopant is obvious. However, same is not true for C-H bond activation.

The study revealed that the most stable adsorption site for methane on TM doped SACs is on the top of the dopant atom. Further, when placed at other sites, methane slides towards the dopant atom after structural optimization. Methane interacts with the partially filled d-bands of the dopant more effectively as compared to the Cu atoms with filled d-band. For all SACs, as we move from left to right of the periodic table, adsorption energy decreases as evident from Fig. 2. However, such a correlation is missing in case of the C-H bondlength elongation. Also, there is no visible one to one correlation between adsorption energies and C-H bond elongation. For all the studied SACs, the range of adsorption energy varies from -0.32 eV to -0.74 eV, and the C-H bondlength elongation scales from 1.101 Å to 1.141 Å as summarized in SI Table 1. Considering Metal-C bondlength and accompanied adsorption energies, we define physisorption at the energy range of -0.10 eV to -0.35 eV and chemisorption at an energy range from -0.35 eV and below (as shown in SI Fig. 1 (A and B)).

Adsorption energy decreases across the period with increasing metal-carbon bondlength as depicted in SI Fig. 1-B. Thus, methane-SAC interactions are dominated by the size, electronegativity, and empty d-states of the dopant atom. Methane is physisorbed on late-transition metal-doped SACs, whereas it is chemisorbed on early-transition and mid-transition metal-doped SACs. Within this range of chemisorption, methane interacts relatively strongly with SACs doped with early-transition metals. This can be attributed to their less electronegativity, more empty d-bands, and large atomic size of the dopant atom. Consequentially, the early-transition metals form metal carbides.<sup>38</sup> Eight of the eighteen transition metals doped SACs reported an elongation of about 3% to 5% in the C-H bond compared to the physisorption on pure Cu(111) surface.

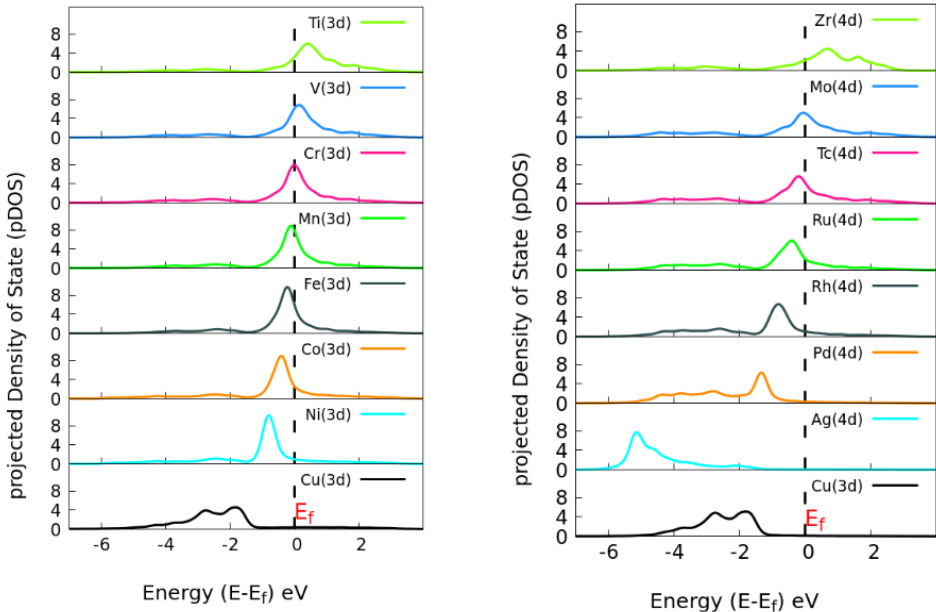


Figure 3: Site specific *pDOS* of various TM doped Cu(111) SACs. *pDOS* for elements with filled d-band lie below Fermi level whereas for SACs with incomplete d-band are near Fermi.

Next, we analyzed the *pDOS* of bare SACs and Cu(111) surfaces, explaining the increased charge transfer in SACs per the dopant atoms. Copper, having its d-states filled, shift towards lower energy whereas SACs with partially empty d-band lie near the Fermi level, as evident from the *pDOS* of the hybridized energy states shown in Fig. 3. Our observations are in line with the d-band center theory, which dictates that the systems with the d-

band center lying near the Fermi level are catalytically more active.<sup>39</sup> Once doped, there is charge redistribution on surface atoms, reported by quantitative Mulliken charge analysis as mentioned in SI Tab. 2.

Interaction between methane and SACs describing the charge transfer from the surface to methane molecule as reported in SI Tab. 2, could be understood from *pDOS* plotted with respect to vacuum and shown in Fig. 4. For isolated methane, C(2p) peak is sharp with the highest intensity. C(2p) peak of physisorbed methane is same in nature but with reduced intensity. C(2p) peak of chemisorbed methane is shown for two cases, the most activated one (Ru/Cu(111)) and the most stable one (Mo/Cu(111)). Not only the peak intensity decreases but also the broadening of the peak along with a secondary peak is observed in both the cases as evident from Fig.4. In addition, our study revealed that the mid-transition doped SACs show more C-H bond activation.

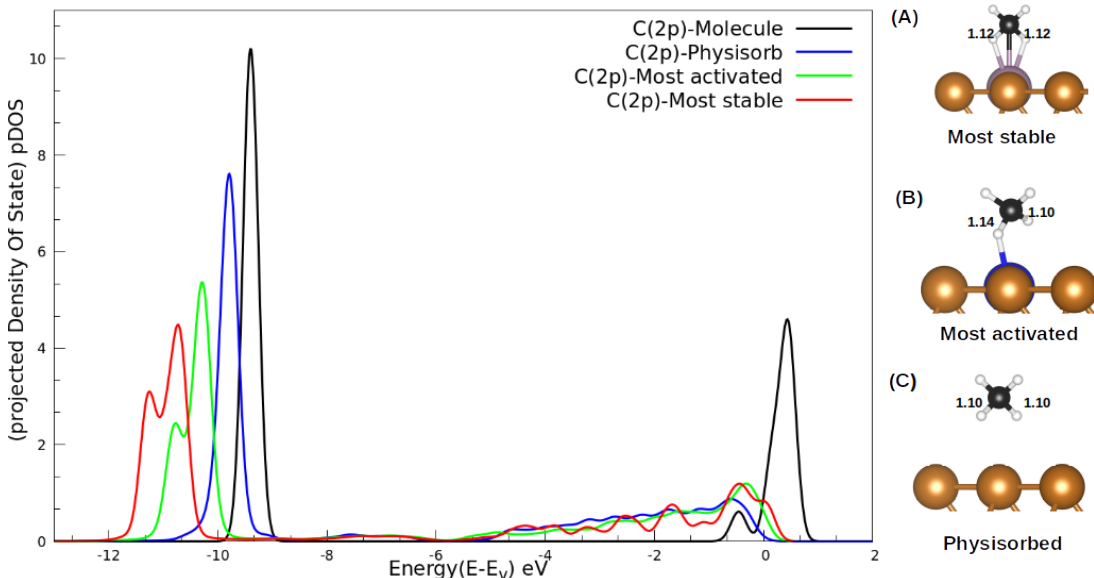


Figure 4: *pDOS* for C(2p) state of methane with respect to vacuum; for molecular (black), physisorbed (blue), most activated (green), and most stable (red). Side panel: (A-C) side view of methane adsorbed on SACs, where copper color is used for Cu, blue for Ru, purple for Mo, white for H and black for the carbon atom

Cleavage of the first C-H bond in CH<sub>4</sub> is a primary and rate determining step for methane conversion towards most value-added products. The SACs which reported a bond elonga-

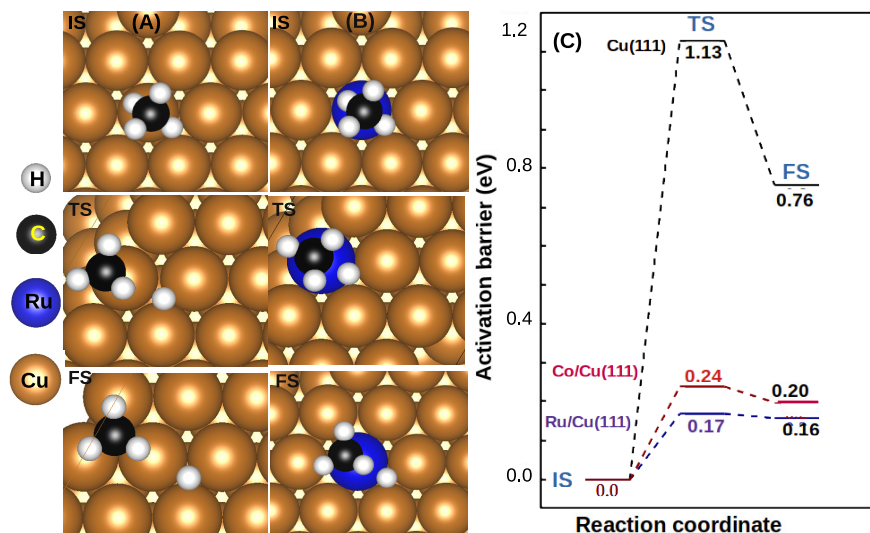


Figure 5: Top view of molecular adsorption (IS), Transition state (TS), and dissociative adsorption (DA/FS) configurations of  $\text{CH}_4$  on: (A)  $\text{Cu}(111)$  surfaces, (B)  $\text{Ru}_1/\text{Cu}(111)$  SACs. Copper, blue, black, and white balls indicate Cu, Ru, C, and H atoms, respectively. Free energy profile of first C-H bond dissociation of  $\text{CH}_4$  on Ru, Co/ $\text{Cu}(111)$ , and  $\text{Cu}(111)$  surfaces.

tion of about 3% - 5% were selected to study dissociative adsorption (DA) of methane. The dissociative adsorption of methane ( $\text{CH}_3 + \text{H}$ ) on  $\text{Cu}(111)$  surface is found to be thermodynamically unfavorable, whereas it is favorable for the SACs. For all the cases studies, dissociation of methane is an endothermic phenomenon, and the values are reported in Table 1. We observed that the lowest activation barrier is accompanied with the most elongated C-H bond. When methane adsorbed strongly, the activation barrier is higher as a result of the formation of a stable configuration (C-M-H sigma complex) as shown in Fig.4-A. Typical configurations of the IS, TS, and FS in case of  $\text{Cu}(111)$  and  $\text{TM}@\text{Cu}(111)$  are shown in Fig. 5, and the relevant data is summarized in Table 1. The ZPE correction is important for C-H bond due to its large vibrational frequency. Computed ZPE for all the SACs is in range of 0.187 to 0.191 eV, which is in agreement with the experimental (0.21 eV) value. Marcinkowski *et al.*,<sup>40</sup> reported the value for C-H bond activation on  $\text{Cu}(111)$  surface,  $E_{ads} = -0.38$  eV, with reaction barrier of 1.4 eV, which is similar to our results,  $E_{ads} = -0.34$  eV,  $E_{act} = 1.32$  eV. Coiobica *et al.*<sup>41</sup> reported that on pure  $\text{Ru}(0001)$  surface the barrier for first C-H bond dissociation is 0.88 eV (85 kJ mol<sup>-1</sup>) for the physisorbed methane. Interestingly,

Table 1: C-H bond activation, M-C bondlength, corresponding adsorption energy (eV) and activation energy for TM/Cu(111) surfaces,  $E_{act}$  with zero point correction and reaction energy

Dopant(TM)	$b_{C-H}$ (Å)	$b_{M-C}$ (Å)	$E_{ads}$ (eV)	$E_{act}$	$E_{act}$ (ZPC)	$E_{rec}$ (eV)
Cu	1.103	3.0	-0.31	1.32	1.13	0.73
Ti	1.121	2.51	-0.63	0.51	0.32	0.06
V	1.124	2.46	-0.61	1.33	1.14	0.22
Fe	1.135	2.45	-0.47	0.67	0.48	0.11
Co	1.130	2.67	-0.41	0.43	0.24	0.20
Ni	1.104	3.0	-0.35	0.49	0.30	0.40
Mo	1.126	2.57	-0.64	1.15	0.96	0.09
Ru	1.141	2.61	-0.51	0.36	0.17	0.16
Rh	1.123	2.90	-0.39	0.45	0.26	0.26

we got significantly smaller activation barrier 0.36 eV, for weakly chemisorbed methane on Ru/Cu(111) SAC. The schematic representation of methane dissociation reaction pathway, bondlength (C-H, Cu-H, Ru-C), activation energy, and reaction energy for the active catalyst is represented in SI Fig. 2. Taking into account the ZPE correction, Ru, Co, and Rh@Cu(111) have the lowest activation barrier. Further, a five fold reduction in the activation barrier is observed for these SACs compared to Cu(111). Thus, Ru, Co, Rh/Cu(111) SACs are efficient catalysts for the first C-H bond dissociation of methane.

## Conclusion

In this work, we have systematically investigated SACs doped with eighteen transition metals on Cu(111) surface as likely candidates for methane activation. We found that on the eighth and ninth group transition-metals doped surfaces viz., Fe, Co, Ru, and Rh possess strong C-H bond activation with moderate adsorption energy and low activation barrier. Interpreting our results, we infer no one-to-one relation between adsorption energies and C-H bond elongation. Our calculations suggest that Ru/Cu(111) is a potential SAC for methane activation, based on its overall structure stability, lower endothermic state, and lower activation

barrier with moderate adsorption energy. While Rh/Cu(111) stands as a promising candidate, authors encourage further investigation into Co/Cu(111), given the cheaper costs of both the constituent metals as compared to other SACs. The low chemical barrier can make methane molecules cleave at low temperatures. In light of practical applications, it would be desirable to investigate further steps for integrated activation and conversion of methane, as a source of hydrogen, direct functionalization, methanol formation, methyl sulphonic acid (CH<sub>3</sub>SO<sub>3</sub>H) formation, halogenation, C-C coupling (higher hydrocarbons, aromatization) and various other unexplored avenues.

## Conflicts of Interests

There are no conflicts to declare.

## Acknowledgements

Authors gratefully acknowledge to CSIR-4PI for computational facility. MB thanks to UGC for the research fellowship.

## References

- (1) Schwach, P.; Pan, X.; Bao, X. Direct conversion of methane to value-added chemicals over heterogeneous catalysts: challenges and prospects. *Chemical reviews* **2017**, *117*, 8497–8520.
- (2) Abbas, H. F.; Daud, W. W. Hydrogen production by methane decomposition: a review. *International journal of hydrogen energy* **2010**, *35*, 1160–1190.
- (3) Marcinkowski, M. D.; Darby, M. T.; Liu, J.; Wimble, J. M.; Lucci, F. R.; Lee, S.; Michaelides, A.; Flytzani-Stephanopoulos, M.; Stamatakis, M.; Sykes, E. C. H. Pt/Cu

- single-atom alloys as coke-resistant catalysts for efficient C–H activation. *Nature chemistry* **2018**, *10*, 325.
- (4) Taccardi, N.; Grabau, M.; Debuschewitz, J.; Distaso, M.; Brandl, M.; Hock, R.; Maier, F.; Papp, C.; Erhard, J.; Neiss, C., et al. Gallium-rich Pd–Ga phases as supported liquid metal catalysts. *Nature chemistry* **2017**, *9*, 862–867.
- (5) Liao, M.-S.; Zhang, Q.-E. Dissociation of methane on different transition metals. *Journal of Molecular Catalysis A: Chemical* **1998**, *136*, 185–194.
- (6) Harris, J.; Simon, J.; Luntz, A. C.; Mullins, C. B.; Rettner, C. T. Thermally assisted tunneling: CH<sub>4</sub> dissociation on Pt(111). *Phys. Rev. Lett.* **1991**, *67*, 652–655.
- (7) Van Santen, R. A. Complementary structure sensitive and insensitive catalytic relationships. *Accounts of chemical research* **2009**, *42*, 57–66.
- (8) Bunnik, B. S.; Kramer, G. J. Energetics of methane dissociative adsorption on Rh {111} from DFT calculations. *Journal of Catalysis* **2006**, *242*, 309–318.
- (9) Bothra, P.; Pati, S. K. Improved catalytic activity of rhodium monolayer modified nickel (110) surface for the methane dehydrogenation reaction: a first-principles study. *Nanoscale* **2014**, *6*, 6738–6744.
- (10) Ang, M.; Miller, J.; Cui, Y.; Mo, L.; Kawi, S. Bimetallic Ni–Cu alloy nanoparticles supported on silica for the water-gas shift reaction: activating surface hydroxyls via enhanced CO adsorption. *Catalysis Science & Technology* **2016**, *6*, 3394–3409.
- (11) Gabrienko, A. A.; Arzumanov, S. S.; Toktarev, A. V.; Danilova, I. G.; Prosvirin, I. P.; Kriventsov, V. V.; Zaikovskii, V. I.; Freude, D.; Stepanov, A. G. Different efficiency of Zn<sup>2+</sup> and ZnO species for methane activation on Zn-modified zeolite. *ACS Catalysis* **2017**, *7*, 1818–1830.

- (12) Rosen, A. S.; Notestein, J. M.; Snurr, R. Q. Structure–Activity Relationships That Identify Metal–Organic Framework Catalysts for Methane Activation. *ACS Catalysis* **2019**, *9*, 3576–3587.
- (13) Fung, V.; Tao, F. F.; Jiang, D.-e. Low-temperature activation of methane on doped single atoms: descriptor and prediction. *Physical Chemistry Chemical Physics* **2018**, *20*, 22909–22914.
- (14) Righi, G.; Magri, R.; Selloni, A. Methane Activation on Metal-Doped (111) and (100) Ceria Surfaces with Charge-Compensating Oxygen Vacancies. *The Journal of Physical Chemistry C* **2020**, *124*, 17578–17585.
- (15) Varghese, J. J.; Trinh, Q. T.; Mushrif, S. H. Insights into the synergistic role of metal–lattice oxygen site pairs in four-centered C–H bond activation of methane: the case of CuO. *Catalysis Science & Technology* **2016**, *6*, 3984–3996.
- (16) Wan, Q.; Fung, V.; Lin, S.; Wu, Z.; Jiang, D.-e. Perovskite-supported Pt single atoms for methane activation. *Journal of Materials Chemistry A* **2020**, *8*, 4362–4368.
- (17) Yang, X.-F.; Wang, A.; Qiao, B.; Li, J.; Liu, J.; Zhang, T. Single-atom catalysts: a new frontier in heterogeneous catalysis. *Accounts of chemical research* **2013**, *46*, 1740–1748.
- (18) Righi, G.; Magri, R.; Selloni, A. Methane Activation on Metal-Doped (111) and (100) Ceria Surfaces with Charge-Compensating Oxygen Vacancies. *The Journal of Physical Chemistry C* **2020**, *124*, 17578–17585.
- (19) Liang, Z.; Li, T.; Kim, M.; Asthagiri, A.; Weaver, J. F. Low-temperature activation of methane on the IrO<sub>2</sub> (110) surface. *Science* **2017**, *356*, 299–303.
- (20) Liu, Y.-C.; Yeh, C.-H.; Lo, Y.-F.; Nachimuthu, S.; Lin, S. D.; Jiang, J.-C. In situ spectroscopic and theoretical investigation of methane activation on IrO<sub>2</sub> nanoparticles: Role of Ir oxidation state on C-H activation. *Journal of Catalysis* **2020**, *385*, 265–273.

- (21) Blöchl, P. E. Projector augmented-wave method. *Physical review B* **1994**, *50*, 17953.
- (22) Kresse, G.; Joubert, D. From ultrasoft pseudopotentials to the projector augmented-wave method. *Physical review b* **1999**, *59*, 1758.
- (23) Perdew, J. P.; Burke, K.; Ernzerhof, M. Generalized gradient approximation made simple. *Physical review letters* **1996**, *77*, 3865.
- (24) Perdew, J. P.; Burke, K.; Ernzerhof, M. Generalized Gradient Approximation Made Simple [Phys. Rev. Lett. 77, 3865 (1996)]. *Physical Review Letters* **1997**, *78*, 1396–1396.
- (25) Kresse, G.; Hafner, J. Ab initio molecular-dynamics simulation of the liquid-metal–amorphous-semiconductor transition in germanium. *Physical Review B* **1994**, *49*, 14251.
- (26) Kresse, G.; Furthmüller, J. Efficient iterative schemes for ab initio total-energy calculations using a plane-wave basis set. *Physical review B* **1996**, *54*, 11169.
- (27) Kresse, G.; Furthmüller, J. Efficiency of ab-initio total energy calculations for metals and semiconductors using a plane-wave basis set. *Computational materials science* **1996**, *6*, 15–50.
- (28) Straumanis, M.; Yu, L. Lattice parameters, densities, expansion coefficients and perfection of structure of Cu and of Cu–In  $\alpha$  phase. *Acta Crystallographica Section A: Crystal Physics, Diffraction, Theoretical and General Crystallography* **1969**, *25*, 676–682.
- (29) Larsen, A. H.; Mortensen, J. J.; Blomqvist, J.; Castelli, I. E.; Christensen, R.; Dułak, M.; Friis, J.; Groves, M. N.; Hammer, B.; Hargus, C., et al. The atomic simulation environment—a Python library for working with atoms. *Journal of Physics: Condensed Matter* **2017**, *29*, 273002.

- (30) Henkelman, G.; Uberuaga, B. P.; Jónsson, H. A climbing image nudged elastic band method for finding saddle points and minimum energy paths. *The Journal of chemical physics* **2000**, *113*, 9901–9904.
- (31) Henkelman, G.; Jónsson, H. Improved tangent estimate in the nudged elastic band method for finding minimum energy paths and saddle points. *The Journal of chemical physics* **2000**, *113*, 9978–9985.
- (32) Henkelman, G.; Jónsson, H. A dimer method for finding saddle points on high dimensional potential surfaces using only first derivatives. *The Journal of chemical physics* **1999**, *111*, 7010–7022.
- (33) Dronskowski, R.; Blöchl, P. E. Crystal orbital Hamilton populations (COHP): energy-resolved visualization of chemical bonding in solids based on density-functional calculations. *The Journal of Physical Chemistry* **1993**, *97*, 8617–8624.
- (34) Deringer, V. L.; Tchougréeff, A. L.; Dronskowski, R. Crystal orbital Hamilton population (COHP) analysis as projected from plane-wave basis sets. *The journal of physical chemistry A* **2011**, *115*, 5461–5466.
- (35) Maintz, S.; Deringer, V. L.; Tchougréeff, A. L.; Dronskowski, R. Analytic projection from plane-wave and PAW wavefunctions and application to chemical-bonding analysis in solids. *Journal of computational chemistry* **2013**, *34*, 2557–2567.
- (36) Maintz, S.; Deringer, V. L.; Tchougréeff, A. L.; Dronskowski, R. LOBSTER: A tool to extract chemical bonding from plane-wave based DFT. *Journal of Computational Chemistry* **2016**, *37*, 1030–1035.
- (37) Qin, F.; Chen, W. Copper-based single-atom alloys for heterogeneous catalysis. *Chemical Communications* **2021**, *57*, 2710–2723.

- (38) Hwu, H. H.; Chen, J. G. Surface chemistry of transition metal carbides. *Chemical reviews* **2005**, *105*, 185–212.
- (39) Nørskov, J. K.; Abild-Pedersen, F.; Studt, F.; Bligaard, T. Density functional theory in surface chemistry and catalysis. *Proceedings of the National Academy of Sciences* **2011**, *108*, 937–943.
- (40) Marcinkowski, M. D.; Darby, M. T.; Liu, J.; Wimble, J. M.; Lucci, F. R.; Lee, S.; Michaelides, A.; Flytzani-Stephanopoulos, M.; Stamatakis, M.; Sykes, E. C. H. Pt/Cu single-atom alloys as coke-resistant catalysts for efficient C–H activation. *Nature chemistry* **2018**, *10*, 325–332.
- (41) Ciobica, I.; Frechard, F.; Van Santen, R.; Kleyn, A.; Hafner, J. A DFT study of transition states for C–H activation on the Ru (0001) surface. *The Journal of Physical Chemistry B* **2000**, *104*, 3364–3369.